Atmospheric
Chemistry
and Physics

Supplement of

Measurement report: Production and loss of atmospheric formaldehyde at a suburban site of Shanghai in summertime

Yizhen Wu et al.

Correspondence to: Qingyan Fu (qingyanf@sheemc.cn) and Lin Wang (lin_wang@fudan.edu.cn)

15 **Text S1. Estimating the contributions of different HCHO sources to ambient HCHO using the ratios of HCHO/C$_2$H$_2$.**

A simple method to estimate contributions of primary HCHO and secondary HCHO, based on the ratios of HCHO and C$_2$H$_2$, is shown in Eq. (S1) (Lin et al., 2012).

$$f_{HCHO} = \left(\left[\frac{HCHO}{C_2H_2}\right]_a - \left[\frac{HCHO}{C_2H_2}\right]_{pri} \right) \Big/ \left[\frac{HCHO}{C_2H_2}\right]_a \qquad (S1)$$

where f_{HCHO} represents the fraction of secondary HCHO, $\left[\frac{HCHO}{C_2H_2}\right]_a$ represents the HCHO-to-C$_2$H$_2$ ratios in the ambient air,

20 and the primary ratio $\left[\frac{HCHO}{C_2H_2}\right]_{pri}$, i.e., the initial mixing ratio of HCHO and C$_2$H$_2$ in the fresh emissions, is assumed to be the

10th percentile value (0.73) of all the measured values of HCHO/C$_2$H$_2$ during our campaign (Wang et al., 2020).

Figure S2 reveals our estimation of average contributions of secondary HCHO during a day. Secondary HCHO exceeded the rest sources including primary and background ones all the time, with the highest values in the afternoon. Secondary HCHO contributed the least to ambient HCHO during 5:00-9:00 LT, whereas at noon and in the afternoon, it showed an obvious

25 enhancement, and then gradually decreased and remained flat during the nighttime. On average, secondary HCHO was estimated to contribute approximately 62.4% to the total ambient HCHO during the campaign, whereas during the time period with the most intensive photochemistry (10:00-16:00 LT), the contribution from secondary HCHO accounted for about 65.7%.

Text S2. Calculation of OH concentrations.

We validated our OH concentration estimation by comparing our estimation in the main text with those obtained by another method (Liu et al., 2020; Fan et al., 2021; Ehhalt and Rohrer, 2000), which takes both photolysis rate and NO_2 concentration into consideration, based on Eq. (S2).

$$c_{OH} = \frac{4.1\times10^9 \times (J_{O^1D})^{0.83} \times (J_{NO_2})^{0.19} \times (140 c_{NO_2}+1)}{0.41 c_{NO_2}^2 + 1.7 c_{NO_2} + 1} \tag{S2}$$

where J_{O^1D} and J_{NO_2} represent photolysis frequencies of O^1D and NO_2, respectively, and c_{NO_2} denotes the concentration of NO_2. The correlation between the results of the method we adopt in the main text and that in Eq. (S2) shows a good agreement (Figure S3), which suggests that our estimation of OH radicals is acceptable.

Text S3. Estimation of NO$_3$ radicals.

HCHO loss due to NO$_3$ radicals is shown as Reaction (RS1), and the loss rate of HCHO by NO$_3$ radicals can thus be expressed as Eq. (S3).

$$\text{HCHO} + NO_3 \rightarrow HNO_3 + HCO \tag{RS1}$$

$$L_{HCHO+NO_3} = [HCHO] \times [NO_3] \times k_{HCHO+NO_3} \tag{S3}$$

We calculated the concentration of NO$_3$ radicals by the method that has been applied in a previous study (Lee et al., 2016), as shown in Eq. (S4).

$$NO_3 = \frac{k_{NO_2+O_3}[NO_2][O_3]}{k_{NO_3+NO}[NO]+k_{NO_3+VOC}+J_{NO_3}} \tag{S4}$$

where k_{NO_3+VOC} is the sum of both the product of the concentration of isoprene and the reaction rate constant for NO$_3$ radicals with isoprene, and that of the concentrations of monoterpenes and the reaction rate constants for NO$_3$ radicals with monoterpenes. Since the only monoterpene we have observed during our campaign was α-pinene, k_{NO_3+VOC} can be expressed by Eq. (S5).

$$k_{NO_3+VOC} = k_{NO_3+isoprene}[isoprene] + k_{NO_3+\alpha-pinene}[\alpha - \text{pinene}] \tag{S5}$$

The estimated concentrations of NO$_3$ radicals are shown in Table S9. The loss rate of HCHO by NO$_3$ radicals was 4 orders of magnitude smaller than that by OH radicals during daytime, and 1-2 orders of magnitude smaller during nighttime when the loss rate of HCHO by OH radicals was small enough to be neglected. Therefore, we conclude that NO$_3$-initiated HCHO removal processes were negligible during the campaign.

55 **Table S1.** The Average, the 10th and the 90th percentile concentrations of trace gases including O_3, NO, NO_2, and C_2H_2, meteorological parameters including photolysis frequencies $J(O^1D)$, J(HCHO_M), J(HCHO_R), wind speed (WS), temperature (Temp), and relative humidity (RH) during the campaign. Note that only photolysis frequencies from sunrise to sunset are considered.

	O_3 (ppbv)	NO (ppbv)	NO_2 (ppbv)	C_2H_2 (ppbv)	$J(O^1D)$ (s^{-1})	J(HCHO_M) (s^{-1})	J(HCHO_R) (s^{-1})	WS (m s^{-1})	Temp (°C)	RH (%)
Average	31	6	14	0.66	1.23×10^{-5}	1.94×10^{-5}	1.36×10^{-5}	1.8	26	83
10th percentile	8	2	7	0.24	1.24×10^{-6}	4.14×10^{-6}	2.63×10^{-6}	0.7	23	62
90th percentile	59	8	23	1.22	3.08×10^{-5}	4.05×10^{-5}	2.95×10^{-5}	3	30	98

60   **Table S2.** Detection limit and accuracy of trace gases, VOCs, photolysis frequencies and BLH.

	Measurement technique	Detection limit	Accuracy (1σ)
HCHO	Aero-Laser formaldehyde monitor	100 pptv	±5%
CH_4	GC-FID	< 100 ppbv	±10%
VOCs [a]	GC-MS/FID	20-300 pptv	±15% to 20%
VOCs [b]	GC-EI-TOF-MS	0.2-7 pptv	±12%
O_3	Ultraviolet photometric analyzer	1 ppbv	±5%
NO, NO_2	Chemiluminescent analyzer	0.40 ppbv	±20%
Photolysis frequencies	Ultra-fast CCD-Detector Spectrometer	/	±5%
BLH	ceilometer	/	±20%

[a] VOCs including propane, *n*-butane, *iso*-butane, *n*-pentane, *iso*-pentane, *n*-hexane, 3-methyl-pentane, *n*-heptane, *n*-octane, *n*-nonane, *n*-Decane, toluene, isoprene, ethene, propene, 1-butene, 1-pentene, *cis*-2-butene, *trans*-2-butene, and 1-hexene.

[b] VOCs including isoprene, α-pinene, MVK and MACR.

65   **Table S3.** The average, standard deviation, maximum and minimum concentrations of the 24 VOC precursors of HCHO during the campaign.

	Average (ppbv)	Standard deviation (ppbv)	Maximum (ppbv)	Minimum (ppbv)	Detector
Methane	2045	166	2760	1676	GC-FID
Propane	2.47	1.84	26.99	0.55	GC-MS/FID
n-Butane	1.25	2.10	43.08	0.18	GC-MS/FID
iso-Butane	1.10	1.45	28.18	0.14	GC-MS/FID
n-Pentane	0.32	0.25	1.55	0.03	GC-MS/FID
iso-Pentane	0.50	0.38	2.53	0.06	GC-MS/FID
n-Hexane	0.24	0.19	1.52	0.02	GC-MS/FID
3-Methyl-pentane	0.12	0.11	1.49	0.02	GC-MS/FID
n-Heptane	0.13	0.28	4.68	0	GC-MS/FID
n-Octane	0.10	0.12	1.48	0.01	GC-MS/FID
n-Nonane	0.03	0.06	0.85	0	GC-MS/FID
n-Decane	0.07	0.20	2.33	0	GC-MS/FID
Toluene	1.70	1.07	4.83	0.26	GC-MS/FID
Isoprene	0.22	0.31	2.81	0	GC-MS/FID, GC-EI-TOF-MS [a]
α-pinene	0.02	0.03	0.32	0	GC-EI-TOF-MS
Ethene	2.18	2.42	16.56	0.12	GC-MS/FID
Propene	0.62	0.75	5.58	0.11	GC-MS/FID
1-butene	0.12	0.10	0.92	0.01	GC-MS/FID
1-pentene	0.05	0.05	0.35	0	GC-MS/FID
cis-2-Butene	0.04	0.04	0.49	0	GC-MS/FID
trans-2-Butene	0.11	0.12	1.07	0.01	GC-MS/FID
1-hexene	0.05	0.06	0.49	0.01	GC-MS/FID
Methyl vinyl ketone	0.28	0.31	2.47	0.02	GC-EI-TOF-MS
Methacrolein	0.08	0.07	0.65	0.01	GC-EI-TOF-MS

[a] This species was detected by both GC-MS/FID and GC-EI-TOF-MS, but quantified in this study by GC-EI-TOF-MS.

Table S4. Reaction rate constants k for reactions of 24 VOC precursors with OH/O_3 and associated HCHO yields.

Species	k with OH [a]	HCHO yield with OH	k with O_3 [a]	HCHO yield with O_3	Reference [b]
Alkanes and Aromatic					
Methane	6.4×10^{-15}	1.0	$<1 \times 10^{-23}$	--	(Atkinson and Arey, 2003; Sumner et al., 2001; IUPAC Task Group; NASA/JPL Data Evaluation)
Propane	1.09×10^{-12}	0.15			(Atkinson and Arey, 2003; Lin et al., 2012; IUPAC Task Group; NASA/JPL Data Evaluation)
n-Butane	2.36×10^{-12}	0.40			(Atkinson and Arey, 2003; Lin et al., 2012; IUPAC Task Group; NASA/JPL Data Evaluation)
iso-Butane	2.2×10^{-12}	0.80			(Lin et al., 2012; IUPAC Task Group; NASA/JPL Data Evaluation)
n-Pentane	3.80×10^{-12}	0.30			(Atkinson and Arey, 2003; Lin et al., 2012; IUPAC Task Group; NASA/JPL Data Evaluation)
iso-Pentane	3.7×10^{-12}	0.50			(Lin et al., 2012; IUPAC Task Group; NASA/JPL Data Evaluation)
n-Hexane	5.20×10^{-12}	0.30			(Atkinson and Arey, 2003; Lin et al., 2012; IUPAC Task Group; NASA/JPL Data Evaluation)

3-Methyl-pentane	5.2×10^{-12}	0.35			(Atkinson and Arey, 2003; Lin et al., 2012; IUPAC Task Group; NASA/JPL Data Evaluation)
n-Heptane	6.76×10^{-12}	0.30			(Atkinson and Arey, 2003; Lin et al., 2012; IUPAC Task Group; NASA/JPL Data Evaluation)
n-Octane	8.11×10^{-12}	0.30			(Atkinson and Arey, 2003; Lin et al., 2012; IUPAC Task Group; NASA/JPL Data Evaluation)
n-Nonane	9.70×10^{-12}	0.30			(Atkinson and Arey, 2003; Lin et al., 2012; IUPAC Task Group; NASA/JPL Data Evaluation)
n-Decane	1.10×10^{-11}	0.30			(Atkinson and Arey, 2003; Lin et al., 2012; IUPAC Task Group; NASA/JPL Data Evaluation)
Toluene	5.63×10^{-12}	0.07			(Atkinson and Arey, 2003; Sumner et al., 2001; IUPAC Task Group; NASA/JPL Data Evaluation)
Alkenes					
Isoprene	1.00×10^{-10}	0.55[c]	1.27×10^{-17}	0.9	(Atkinson and Arey, 2003; Choi et al., 2010; IUPAC Task Group; NASA/JPL Data Evaluation)

α-pinene	5.23×10^{-11}	0.19	8.4×10^{-17}	0.25	(Atkinson and Arey, 2003; Choi et al., 2010; IUPAC Task Group; NASA/JPL Data Evaluation)
Ethene	8.52×10^{-12}	1.8	1.59×10^{-18}	1.03	(Atkinson and Arey, 2003; Choi et al., 2010; IUPAC Task Group; NASA/JPL Data Evaluation)
Propene	2.63×10^{-11}	1.0	1.01×10^{-17}	0.78	(Atkinson and Arey, 2003; Choi et al., 2010; IUPAC Task Group; NASA/JPL Data Evaluation)
1-Butene	3.14×10^{-11}	1.0	9.64×10^{-18}	0.63	(Atkinson and Arey, 2003; Sumner et al., 2001; IUPAC Task Group; NASA/JPL Data Evaluation)
1-Pentene	3.14×10^{-11}	0.5	1.06×10^{-17}	0.55	(Atkinson and Arey, 2003; Lee et al., 1998; Sumner et al., 2001; IUPAC Task Group; NASA/JPL Data Evaluation)
cis-2-Butene	5.64×10^{-11}	0.0	1.25×10^{-16}	0.126	(Atkinson and Arey, 2003; Lin et al., 2012; Grosjean and Grosjean, 1996; IUPAC Task Group; NASA/JPL Data Evaluation)
trans-2-Butene	6.40×10^{-11}	0.0	1.90×10^{-16}	0.126	(Atkinson and Arey, 2003; Lin et al., 2012; Grosjean and Grosjean, 1996;

					IUPAC Task Group; NASA/JPL Data Evaluation)
1-Hexene	3.7×10^{-11}	0.5	1.13×10^{-17}	0.50	(Atkinson and Arey, 2003; Lee et al., 1998; Grosjean and Grosjean, 1996; IUPAC Task Group; NASA/JPL Data Evaluation)
OVOCs					
Methyl vinyl ketone	2.0×10^{-11}	0.58	5.2×10^{-18}	0	(Atkinson and Arey, 2003; Sumner et al., 2001; IUPAC Task Group; NASA/JPL Data Evaluation)
Methacrolein	2.9×10^{-11}	0.61	1.2×10^{-18}	0	(Atkinson and Arey, 2003; Choi et al., 2010; IUPAC Task Group; NASA/JPL Data Evaluation)

70   [a] The unit of k is cm^3 molecule^{-1} s^{-1}.

[b] IUPAC Task Group on Atmospheric Chemical Kinetic Data Evaluation, available at https://iupac-aeris.ipsl.fr/index.html#, last access: 23 September 2022;

NASA/JPL Data Evaluation, available at http://jpldataeval.jpl.nasa.gov/, last access: 22 September 2022.

[c] HCHO yield from isoprene does not include those from its oxidation products such as MVK and MACR.

75

Table S5. The estimated Average, standard deviation, and the 10th and the 90th percentile concentrations of OH radicals during the campaign. Note that only concentrations of OH radicals from sunrise to sunset are considered.

	Average (molecules cm^{-3})	Standard deviation (molecules cm^{-3})	10th percentile (molecules cm^{-3})	90th percentile (molecules cm^{-3})
OH	3.69×10^6	3.22×10^6	3.71×10^5	9.25×10^6

80   **Table S6.** Calculated uncertainties of HCHO production rates and associated uncertainties in measurements of 24 VOCs and ozone, estimations of OH, reaction rate coefficients and corresponding HCHO yields for reactions between VOCs and oxidants.

	The sunny period	The cloudy and rainy period
	(%)	(%)
Methane	0.3	0.3
Propane	2.4	2.5
n-Butane	3.3	2.2
iso-Butane	3.4	2.3
n-Pentane	3.2	2.5
iso-Pentane	3.0	2.3
n-Hexane	2.8	2.7
3-Methyl-pentane	3.1	2.7
n-Heptane	4.2	4.6
n-Octane	3.3	3.6
n-Nonane	4.0	3.3
n-Decane	5.2	4.3
Toluene	1.9	2.1
Isoprene	3.1	3.4
α-pinene	3.1	3.8
Ethene	3.8	3.8
Propene	2.8	3.5
1-Butene	2.9	2.6
1-Pentene	3.7	3.4
cis-2-Butene	3.1	2.4
trans-2-Butene	3.2	2.6
1-Hexene	3.1	2.6
Methyl vinyl ketone	2.5	2.6
Methacrolein	3.4	3.1
OH	20	
O_3	5	
k with OH [a]	2	
k with O_3 [a]	2	

HCHO yields	2	
Total	25.9	21.0

[a] IUPAC Task Group on Atmospheric Chemical Kinetic Data Evaluation, available at https://iupac-aeris.ipsl.fr/index.html#, last access: 23 September 2022;

NASA/JPL Data Evaluation, available at http://jpldataeval.jpl.nasa.gov/, last access: 22 September 2022.

85

Table S7. Calculated uncertainties of HCHO loss rates and associated uncertainties in measurements of HCHO, photolysis frequencies, and BLH, and estimations of OH, and reaction rate coefficients for reactions between VOCs and OH.

	The sunny period (%)	The cloudy and rainy period (%)
HCHO	2.9	2.9
Photolysis frequencies	5	
BLH	20	
OH	20	
k with OH	2	
Total	28.9	28.9

90 **Table S8.** Uncertainties of the calculated net HCHO production rates and the observed rates of HCHO concentration change during the sunny period and the cloudy and rainy period.

	The sunny period (%)	The cloudy and rainy period (%)
Calculated net HCHO production rates	38.8	35.7
Observed rates of HCHO concentration change	30	30

The sunny period (%)   The cloudy and rainy period (%)

Table S9. The estimated average, standard deviation, and the 10th and the 90th percentile concentrations of NO_3 radicals.

	Average (molecules cm^{-3})	Standard deviation (molecules cm^{-3})	10th percentile (molecules cm^{-3})	90th percentile (molecules cm^{-3})
NO_3	3.24×10^6	2.59×10^6	7.51×10^5	6.68×10^6

95
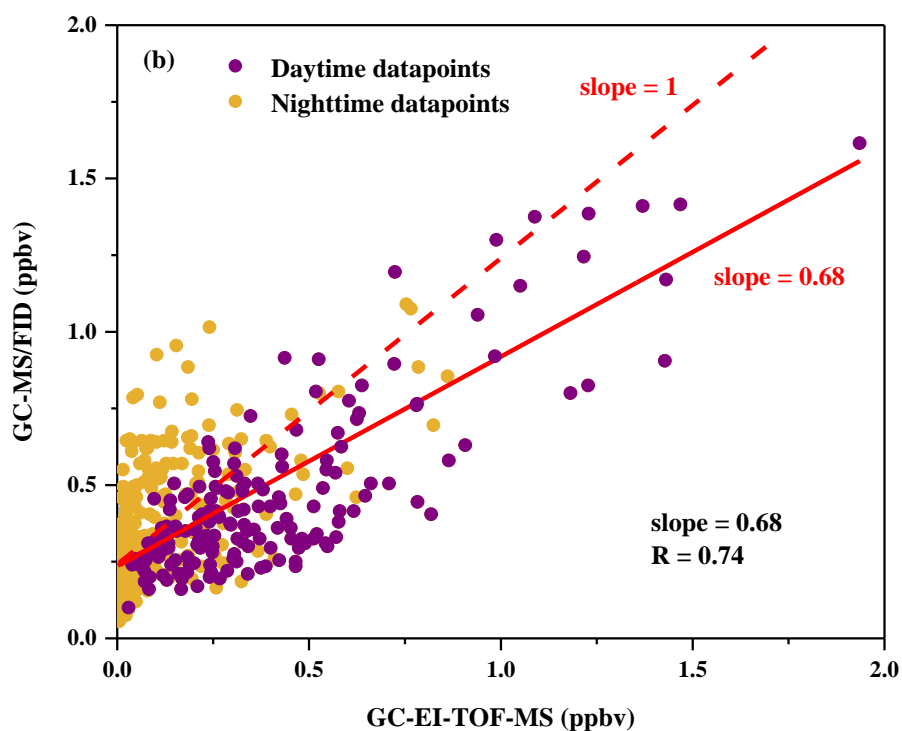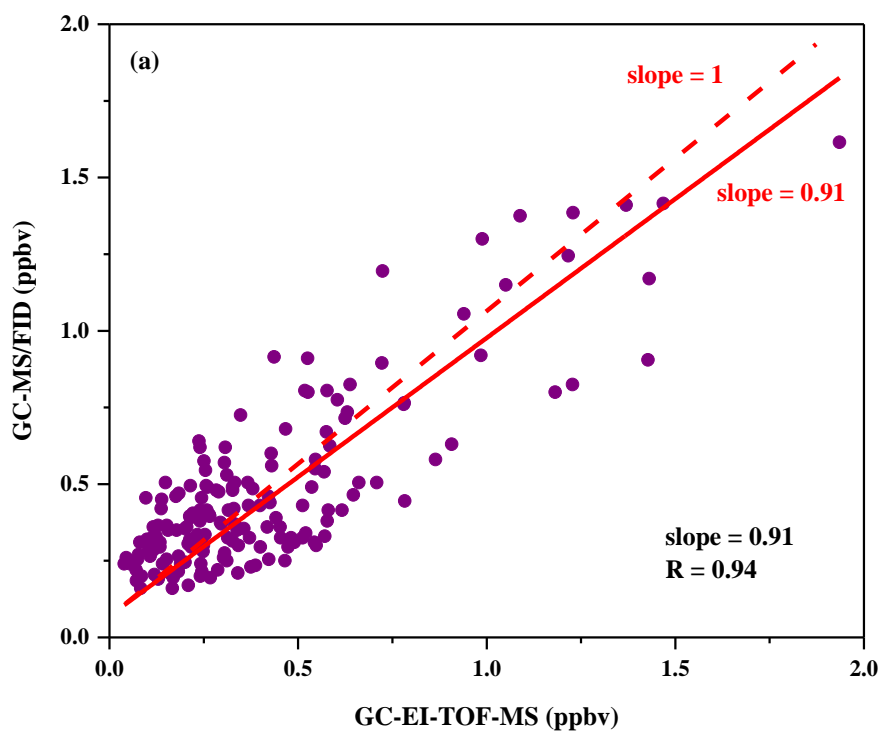
Figure S1. Inter-comparison of isoprene between GC-EI-TOF-MS and GC-MS/FID. The purple circles show the measured daytime concentrations, the yellow circles represent the measured nighttime concentrations, the red solid lines denote the best linear fits, and the red dashed lines represent a 1:1 line for comparison. (a) Isoprene concentrations during daytime (10:00~16:00); (b) isoprene concentrations during the whole campaign.
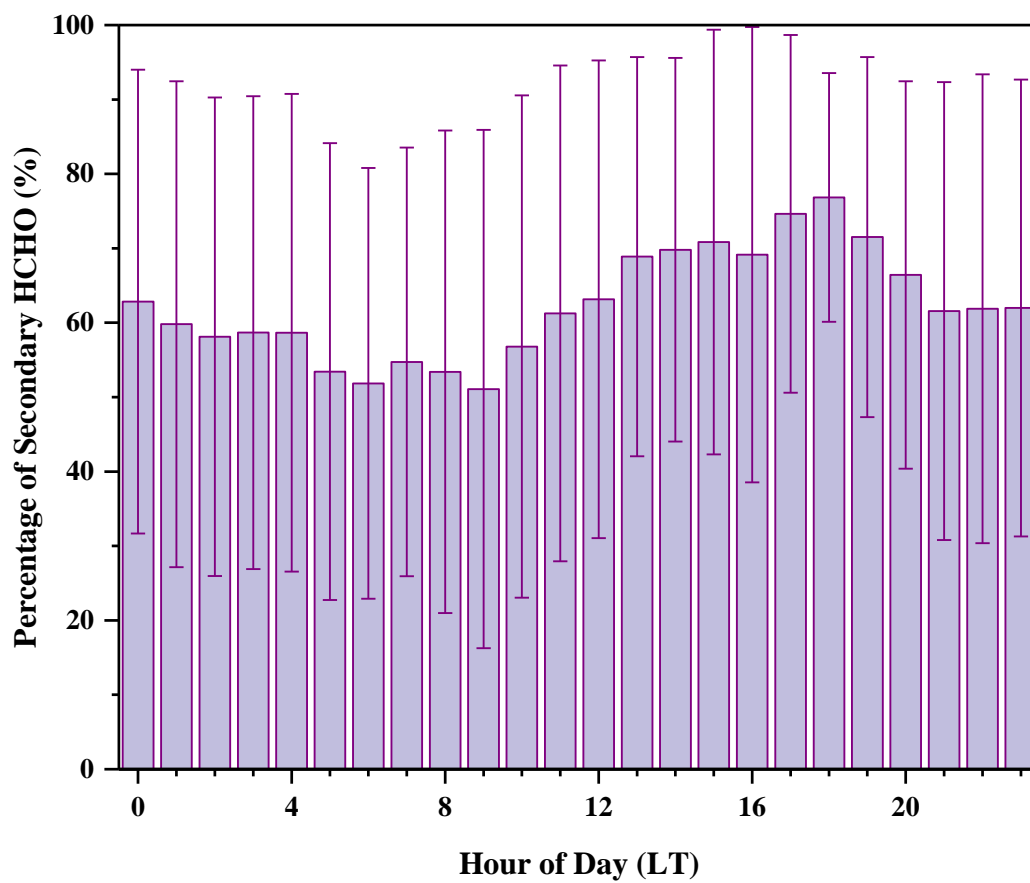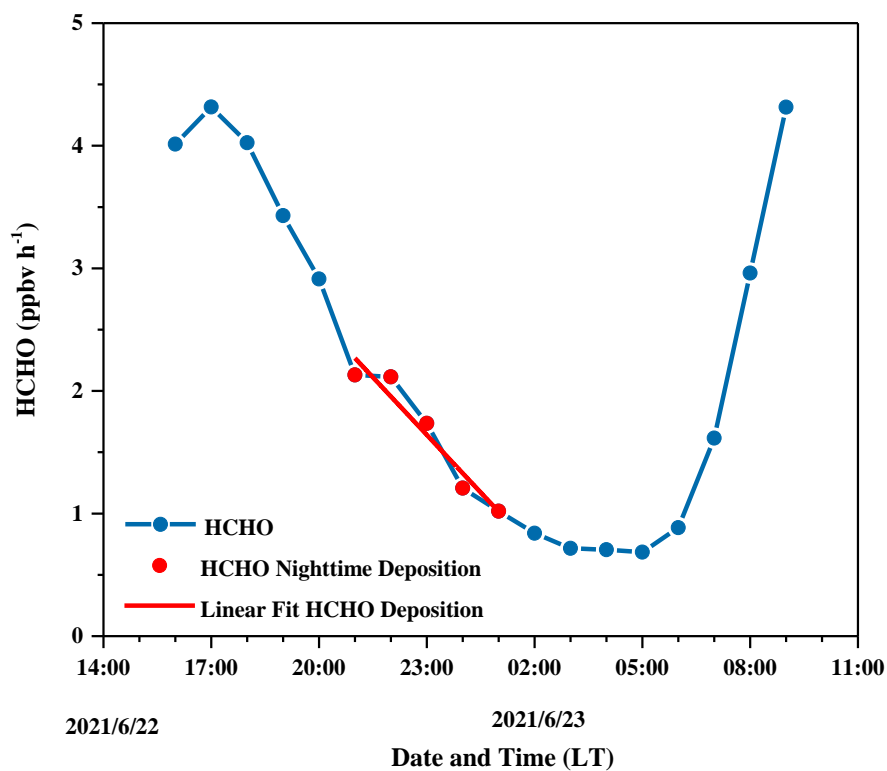
Figure S2. Diurnal contributions of secondary HCHO based on emission ratios of HCHO-to-C_2H_2, with the error bar representing one standard deviation.
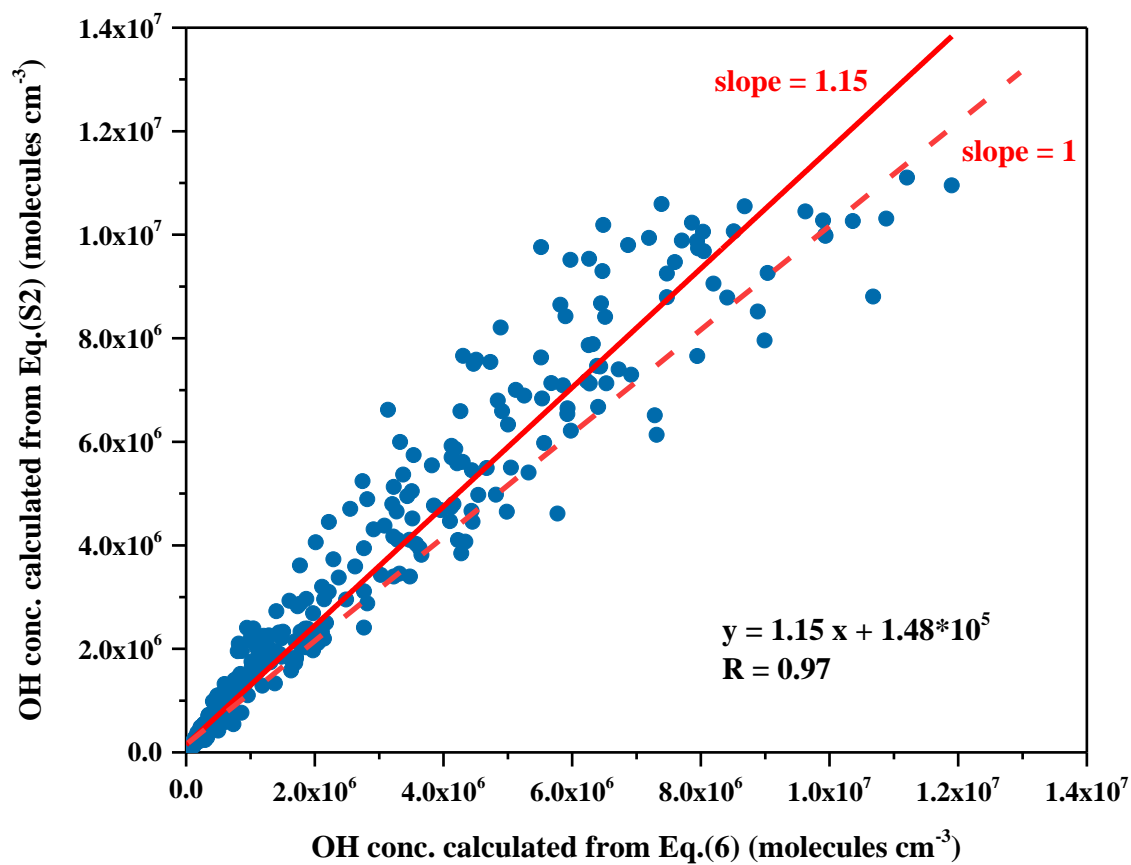
Figure S3. Correlation between the concentration of OH based on different calculation methods. The red solid line denotes the best linear fit, and the red dashed line represents a 1:1 line for comparison.

110

Figure S4. Determination of the deposition velocity based on the HCHO nighttime loss, which is here exemplarily shown for one night during the campaign. Blue data points represent the HCHO mixing ratios, the red color highlights the data points which we included in our nighttime HCHO loss analysis and the red line is the linear fit of these data points.

115
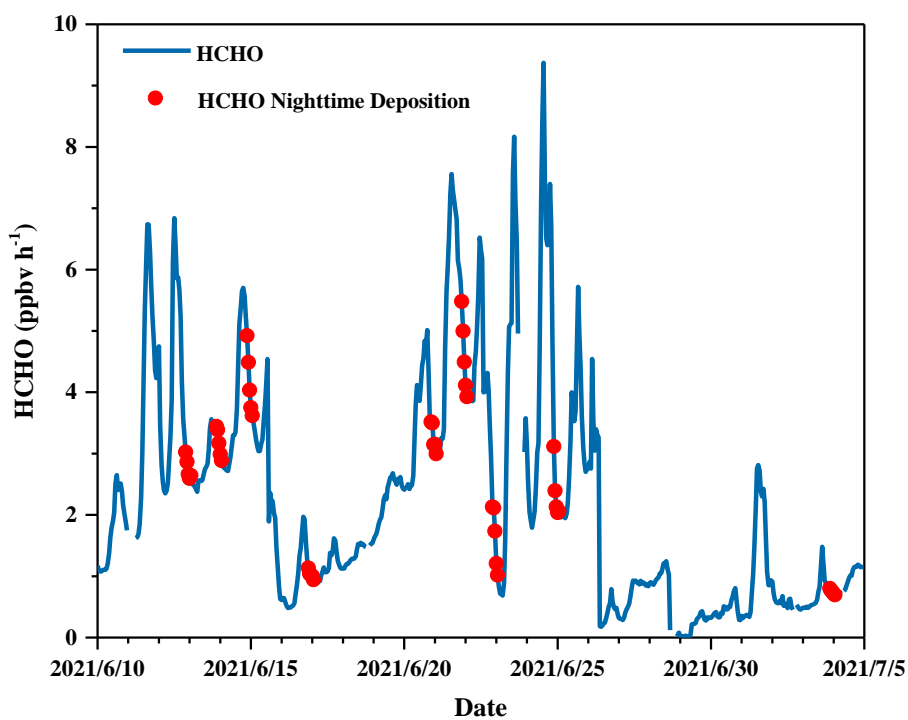
Figure S5. The temporal development of the HCHO concentration during the campaign. The red data points (5 for each night) are used for determining the HCHO deposition velocity at nighttime.
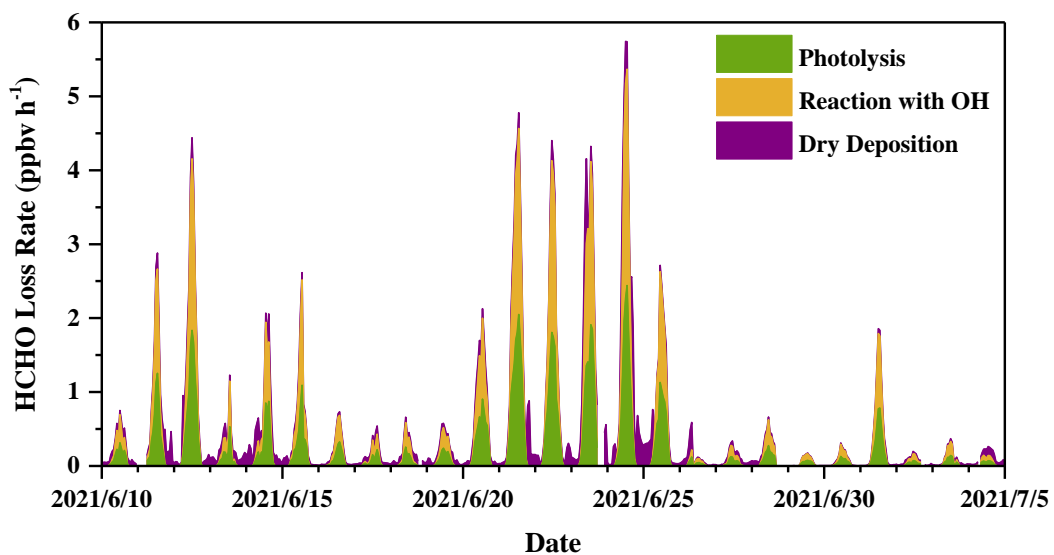
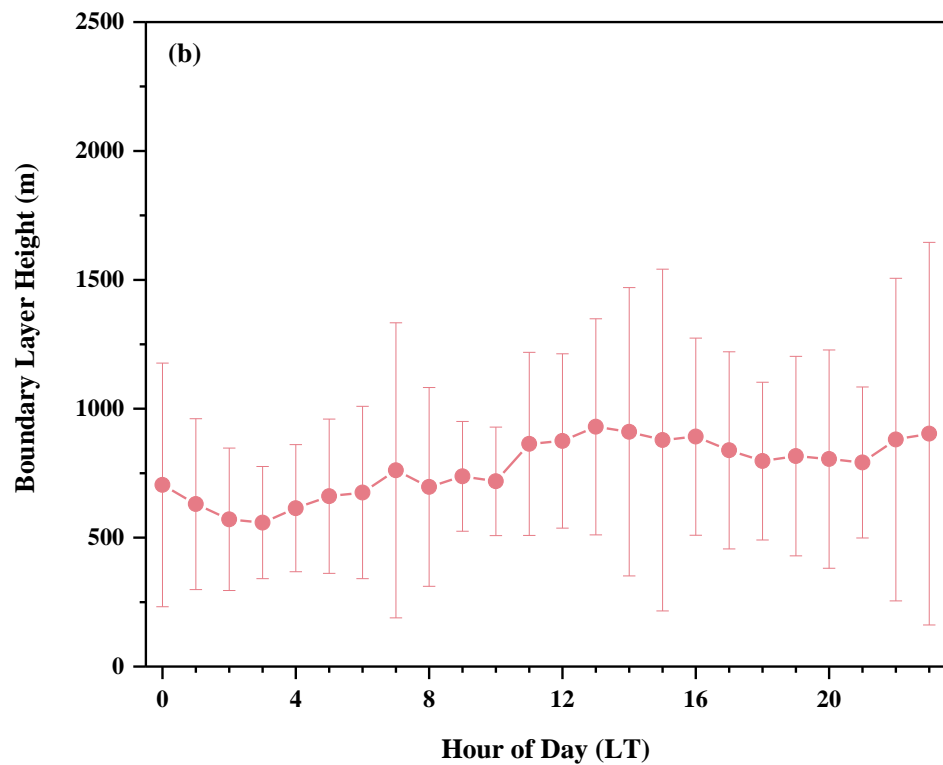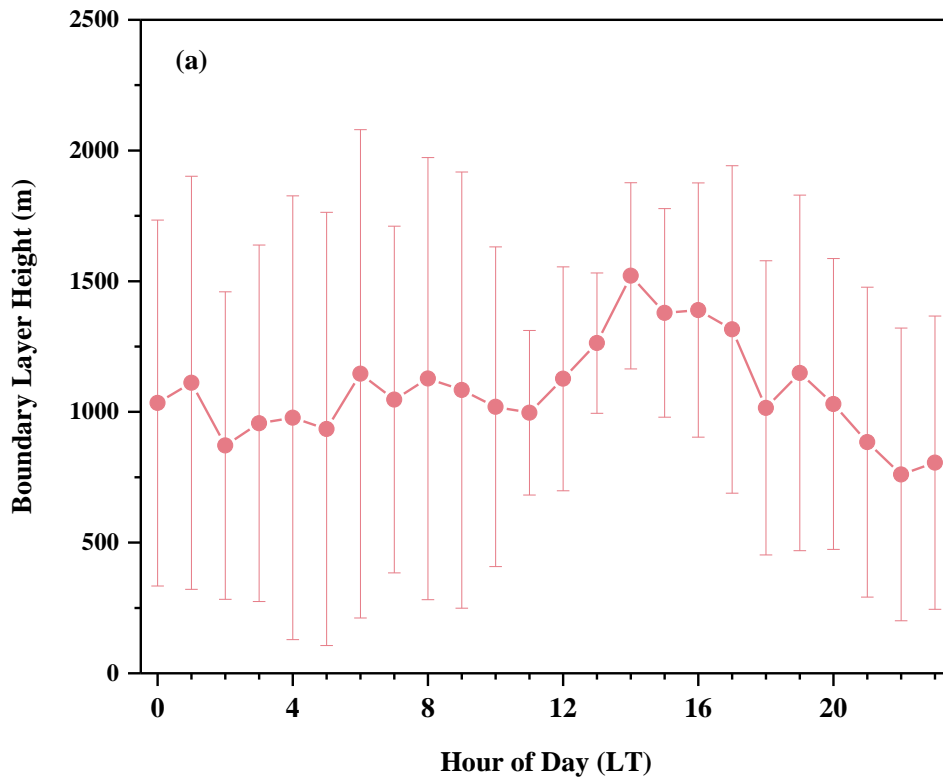**Figure S6. Time profiles of the calculated HCHO loss rates during the campaign.**

120

Figure S7. Average diurnal profile of Boundary Layer Height (BLH) in (a) the sunny period and (b) the cloudy and rainy period, respectively, with the error bar representing one standard deviation.

References

Atkinson, R. and Arey, J.: Atmospheric Degradation of Volatile Organic Compounds, Chem. Rev., 103, 4605–4638, https://doi.org/10.1021/cr0206420, 2003.

Choi, W., Faloona, I. C., Bouvier-Brown, N. C., McKay, M., Goldstein, A. H., Mao, J., Brune, W. H., LaFranchi, B. W., Cohen, R. C., Wolfe, G. M., Thornton, J. A., Sonnenfroh, D. M., and Millet, D. B.: Observations of elevated formaldehyde over a forest canopy suggest missing sources from rapid oxidation of arboreal hydrocarbons, Atmos. Chem. Phys., 10, 8761–8781, https://doi.org/10.5194/acp-10-8761-2010, 2010.

Ehhalt, D. H. and Rohrer, F.: Dependence of the OH concentration on solar UV, J. Geophys. Res. Atmos., 105, 3565–3571, https://doi.org/10.1029/1999JD901070, 2000.

Fan, X., Cai, J., Yan, C., Zhao, J., Guo, Y., Li, C., Dällenbach, K. R., Zheng, F., Lin, Z., Chu, B., Wang, Y., Dada, L., Zha, Q., Du, W., Kontkanen, J., Kurtén, T., Iyer, S., Kujansuu, J. T., Petäjä, T., Worsnop, D. R., Kerminen, V. M., Liu, Y., Bianchi, F., Tham, Y. J., Yao, L., and Kulmala, M.: Atmospheric gaseous hydrochloric and hydrobromic acid in urban Beijing, China: Detection, source identification and potential atmospheric impacts, Atmos. Chem. Phys., 21, 11437–11452, https://doi.org/10.5194/acp-21-11437-2021, 2021.

Grosjean, E. and Grosjean, D.: Carbonyl products of the gas-phase reaction of ozone with 1-alkenes, Environ. Sci. Technol., 30, 4107–4113, https://doi.org/10.1016/1352-2310(96)00176-8, 1996.

Lee, B. H., Mohr, C., Lopez-Hilfiker, F. D., Lutz, A., Hallquist, M., Lee, L., Romer, P., Cohen, R. C., Iyer, S., Kurtén, T., Hu, W., Day, D. A., Campuzano-Jost, P., Jimenez, J. L., Xu, L., Ng, N. L., Guo, H., Weber, R. J., Wild, R. J., Brown, S. S., Koss, A., De Gouw, J., Olson, K., Goldstein, A. H., Seco, R., Kim, S., McAvey, K., Shepson, P. B., Starn, T., Baumann, K., Edgerton, E. S., Liu, J., Shilling, J. E., Miller, D. O., Brune, W., Schobesberger, S., D'Ambro, E. L., and Thornton, J. A.: Highly functionalized organic nitrates in the southeast United States: Contribution to secondary organic aerosol and reactive nitrogen budgets, Proc. Natl. Acad. Sci. U. S. A., 113, 1516–1521, https://doi.org/10.1073/pnas.1508108113, 2016.

Lee, Y. N., Zhou, X., Kleinman, L. I., Nunnermacker, L. J., Springston, S. R., Daum, P. H., Newman, L., Keigley, W. G., Holdren, M. W., Spicer, C. W., Young, V., Fu, B., Parrish, D. D., Holloway, J., Williams, J., Roberts, J. M., Ryerson, T. B., and Fehsenfeld, F. C.: Atmospheric chemistry and distribution of formaldehyde and several multioxygenated carbonyl compounds during the 1995 Nashville/Middle Tennessee Ozone Study, J. Geophys. Res. Atmos., 103, 22449–22462, https://doi.org/10.1029/98JD01251, 1998.

Lin, Y. C., Schwab, J. J., Demerjian, K. L., Bae, M.-S. S., Chen, W.-N. N., Sun, Y., Zhang, Q., Hung, H.-M. M., and Perry, J.: Summertime formaldehyde observations in New York City: Ambient levels, sources and its contribution to HOx radicals, J. Geophys. Res. Atmos., 117, 1–14, https://doi.org/10.1029/2011JD016504, 2012.

Liu, Y., Zhang, Y., Lian, C., Yan, C., Feng, Z., Zheng, F., Fan, X., Chen, Y., Wang, W., Chu, B., Wang, Y., Cai, J., Du, W., R. Daellenbach, K., Kangasluoma, J., Bianchi, F., Kujansuu, J., Petäjä, T., Wang, X., Hu, B., Wang, Y., Ge, M., He, H., and Kulmala, M.: The promotion effect of nitrous acid on aerosol formation in wintertime in Beijing: The possible contribution of traffic-related emissions, Atmos. Chem. Phys., 20, 13023–13040, https://doi.org/10.5194/acp-20-13023-2020, 2020.

Sumner, A. L., Shepson, P. B., Couch, T. L., Thornberry, T., Carroll, M. A., Sillman, S., Pippin, M., Bertman, S., Tan, D., Faloona, I., Brune, W., Young, V., Cooper, O., Moody, J., and Stockwell, W.: A study of formaldehyde chemistry above a forest canopy, J. Geophys. Res. Atmos., 106, 24387–24405, https://doi.org/10.1029/2000JD900761, 2001.

Wang, H., Wang, Q., Gao, Y., Zhou, M., Jing, S., Qiao, L., Yuan, B., Huang, D., Huang, C., Lou, S., Yan, R., de Gouw, J. A., Zhang, X., Chen, J., Chen, C., Tao, S., An, J., and Li, Y.: Estimation of Secondary Organic Aerosol Formation During a Photochemical Smog Episode in Shanghai, China, J. Geophys. Res. Atmos., 125, 1–14, https://doi.org/10.1029/2019JD032033, 2020.